Nanoscale Research Letters

NANO EXPRESS

Open Access

Significant Detectivity Enhancement of Broad Spectral Organic–Inorganic Hybrid Photodiodes by C_{60} Film as Hole-Blocking Layer

Zhuoli Zhou[1], Guangmeng Liao[2], Xinyu Song[1], Qinyong Dai[1], Lei Sun[1*], Yingquan Peng[1,2*] and Peng Wang[2]

Abstract

As an important classification of photodetectors, broad spectral photodiodes are ubiquitous in the fields of industry and scientific research. Here, we reported a type of broad spectral organic–inorganic hybrid photodiodes (OIHPDs) based on planar-bulk heterojunction, which composed of 3,4,9,10-perylenetertracarboxylic dianhydride (PTCDA), copper phthalocyanine (CuPc) and fullerene (C_{60}). In our research, the dark current of the OIHPD with 10 nm C_{60} film (10 nm-C_{60} OIHPD) was as low as 25.6 μA, which is about 63 times smaller than the dark current of the OIHPD without C_{60} film (C_{60}-free OIHPD). It is considered that the significantly enhanced performance of 10 nm-C_{60} OIHPD is attributed to the introduction of the C_{60} film, which act as hole-blocking layer to reduce the dark current. And through the schematic energy level model combined with experimental measurements, the reason for the dark current change was well explained. Furthermore, the specific detectivity of 10 nm-C_{60} OIHPD was almost one order of magnitude larger than it of C_{60}-free OIHPD, and a notable enhancement of over 10^{11} cm $Hz^{1/2}$/W was obtained due to the fiercely reduced dark current. These results provide insights on how to improve the performance of organic photodiodes.

Keywords: Broad spectral photodiodes, Organic–inorganic hybrid photodiodes, Planar-bulk heterojunction, Hole-blocking layer

Introduction

In optical information transmission and processing, photodetectors, which convert optical signals into electrical signals, are critical devices, especially in optical fiber communication [1], night vision [2], infrared remote sensing [3], imaging [4, 5], biomedical [6] and spectrometer [7]. At present, conventional inorganic photodetectors based on Gallium nitride (GaN), silicon (Si) and indium gallium arsenide (InGaAs) were well developed for detecting different sub-bands within the ultraviolet to near infrared range [8–10]. However, the flexibility of inorganic semiconductor materials is not satisfactory. Furthermore, some photodetectors based on inorganic semiconductor materials must be cooled during operation [11], which greatly restrict its further development and practical application. Thus, organic semiconductor materials have attracted widespread attention from researchers due to their good compatibility and special physical properties [12–15]. The development of organic–inorganic hybrid structures and the optimization of multicomponent organic heterojunctions are always good ideas for achieving broad spectral response through the complementarity of absorption spectra between different materials [16, 17]. For example, Yang et al. fabricated an organic photodetector with broad spectral photo-response from 200 to 1000 nm by adopting thick polymer bulk heterojunction composed of 1, 1-bis ((di-4-tolylamino) phenyl) cyclohexane (TAPC) and C_{70}, and achieved an external quantum efficiency (*EQE*) over 1000%, a specific detectivity (D^*) over 10^{11} Jones (cm $Hz^{1/2}$/W) [18]. Wang et al. reported a mixed

*Correspondence: 17a0403150@cjlu.edu.cn; yqpeng@cjlu.edu.cn
[1] College of Optical and Electronic Technology, China Jiliang University, Hangzhou 310018, China
Full list of author information is available at the end of the article

Springer Open

© The Author(s) 2022. **Open Access** This article is licensed under a Creative Commons Attribution 4.0 International License, which permits use, sharing, adaptation, distribution and reproduction in any medium or format, as long as you give appropriate credit to the original author(s) and the source, provide a link to the Creative Commons licence, and indicate if changes were made. The images or other third party material in this article are included in the article's Creative Commons licence, unless indicated otherwise in a credit line to the material. If material is not included in the article's Creative Commons licence and your intended use is not permitted by statutory regulation or exceeds the permitted use, you will need to obtain permission directly from the copyright holder. To view a copy of this licence, visit http://creativecommons.org/licenses/by/4.0/.

tin–lead perovskites ($MASn_{1-x}Pb_xI_3$) photodetectors by using low-bandgap $(FASnI_3)_{0.6}(MAPbI_3)_{0.4}$ perovskite (FA = formamidinium) as the active layer, and achieved an *EQE* larger than 65% under − 0.2 V bias, a D^* of $10^{11} \sim 10^{12}$ Jones in the wavelength range of 350–900 nm [19]. Han et al. developed a polymer photodetector by inserting cathode and anode interlayers, and achieved a D^* over 10^{12} Jones in the wavelength range of 300–1700 nm [20]. Ma et al. utilized a ZnO/In_2O_3 heterojunction to improve sensing performance [21]. Zhang et al. fabricated a asymmetric supercapacitors with high energy density by using 3D hierarchical $CoWO_4/Co3O_4$ nanowire arrays [22]. And core–shell heterostructures were also used in nano structures [23]. Recently, our group has also demonstrated some broad spectral organic photodetectors based on planar heterojunction or hybrid planar-bulk heterojunction [24–26]. In addition, organic photodetectors have the advantages of low cost, high flexibility and large-area scalability, which make organic photodetectors have special research value and broad application prospects in the traditional optoelectronic field [27–30].

Generally speaking, the broad spectral photodetectors can be classified into three categories: phototransistors, photodiodes and photoconductors, and the structures include planar structure, bulk heterostructure and hybrid structure [31–33]. With further research, a series of methods have been adopted to improve the performance of organic photodetectors, such as developing new materials, optimizing device structure, doping quantum dots and inserting the inducing layers [34–38]. In this paper, we reported the broad spectral organic–inorganic hybrid photodiodes (OIHPDs) based on planar-bulk heterojunction of Si/C_{60}/3,4,9,10-perylenetertracarboxylic dianhydride: copper phthalocyanine (PTCDA:CuPc) /Au. C_{60} presents numerous exciting chemical and physical properties and has been widely employed as an efficient trapping material in various optoelectronic applications. It is worth mentioning that the C_{60} film was introduced as a hole-blocking layer to enhance the barrier height for blocking hole transport. Thereby, the dark current was significantly reduced, and the spectral response was covered from visible light to near-infrared using PTCDA:CuPc as a light absorbing layer. The resulting organic photodetectors showed a specific detectivity over 10^{11} Jones in the spectral range of 405–655 nm.

Methods

Fabrication of Devices

The device configuration of the OIHPDs is depicted in Fig. 1, in which P-type silicon was used as the substrates, C_{60} films as buffer layers, organic bulk heterojunction as photosensitive layers and gold films as the top electrodes.

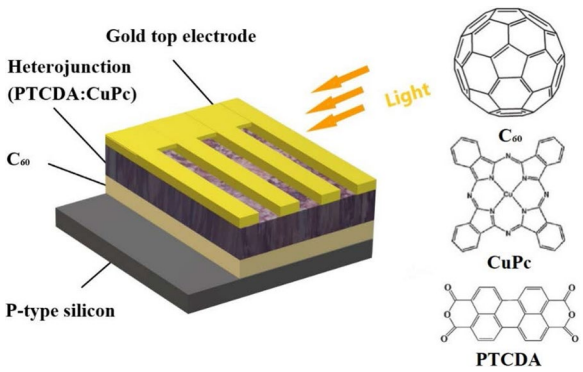

Fig. 1 The schematic structure of devices based on hybrid planar-bulk heterojunction. The insets are molecular structures of PTCDA, CuPc and C_{60}

Furthermore, the molecular structures of the organic materials are also inserted into Fig. 1 to understand the principle of the devices. For device fabrication, the p-type silicon substrates were successively cleaned by acetone, alcohol and deionized water for 10 min each, and then dried with floating N_2 gas and baked in a vacuum oven at 60 °C for 20 min. Through a quartz crystal oscillator, it can monitor the different thickness of the films, and control the baffle and shadow masks, different thicknesses C_{60} ($\delta = 0$, 5, 10, 20 and 30 nm, δ is the C_{60} thickness) films were deposited on the cleaned p-type silicon substrates by vacuum thermal evaporation. Following that, 30 nm-thick PTCDA:CuPc (weight ratio 1: 1, both purchased from Aladdin Biochemical Technology Co., Ltd.) bulk heterojunction films were vacuum evaporated on the top of C_{60} films. Next, the gold top electrodes were deposited on the organic films by shadow masks. During the deposition process, the chamber pressure was maintained below 3×10^{-4} Pa and the evaporation rate was kept at 0.1–0.2 Å/s. The effective area of each photodetector is 0.06 cm^2.

Characterization of Devices

The absorption spectra of films were measured by using TU-1901 spectrometer. All measurements were performed using a semiconductor characterization system in a dark chamber at room temperature. Laser diodes with wavelengths of 405 nm, 450 nm, 532 nm, 655 nm and 808 nm were used as the light source, and the different optical powers were realized by using neutral density filters.

Results and Discussion

Figure 2a depict the optical absorption spectra of 30 nm-thick PTCDA:CuPc films on different thicknesses C_{60} films and C_{60} single layer. Here, the PTCDA:CuPc films

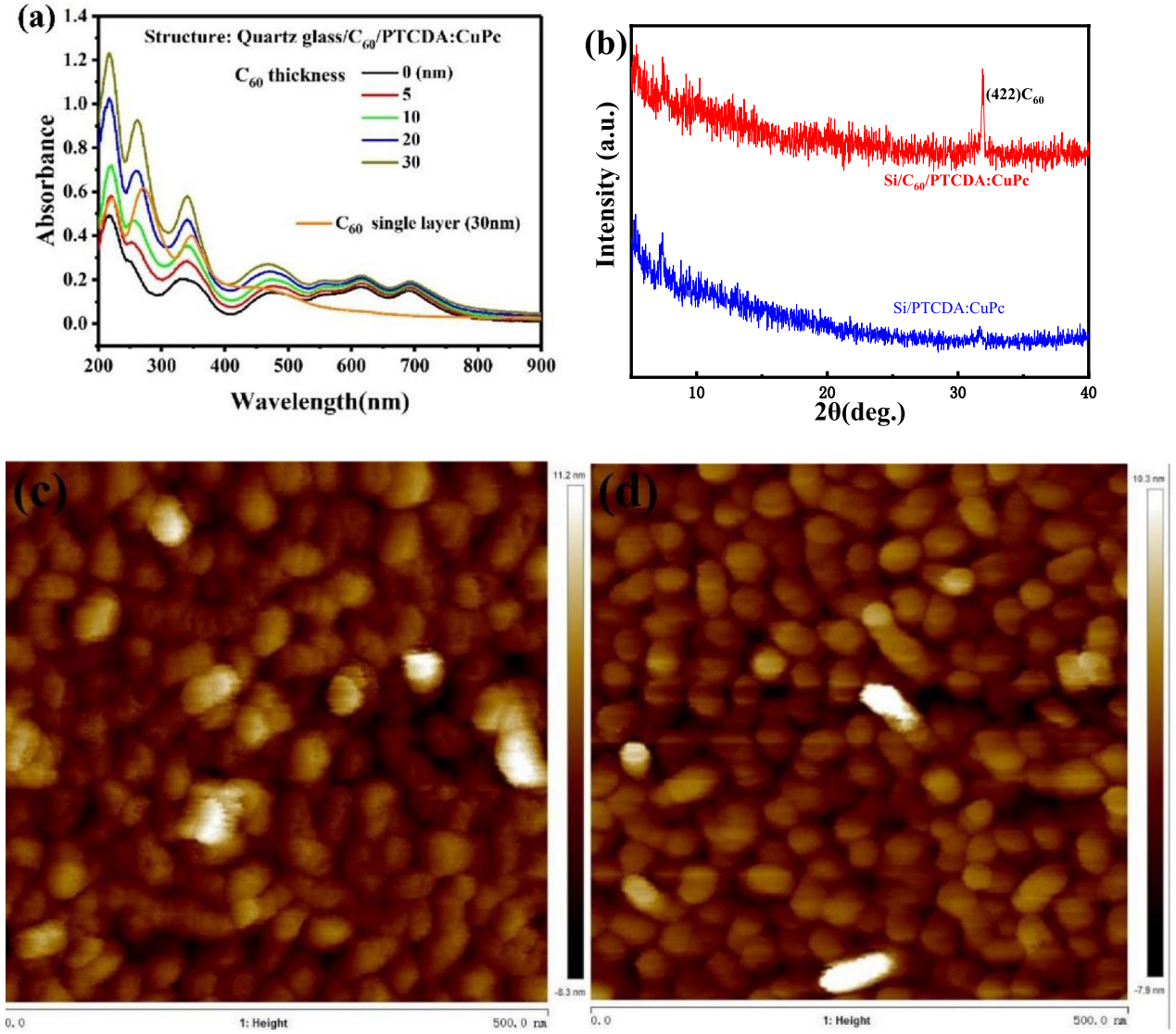

Fig. 2 **a** Optical absorption spectra of C_{60} single layer (30 nm) and PTCDA:CuPc (30 nm) films deposited on C_{60} film of different thicknesses. All films were deposited on quartz glasses. **b** XRD spectrum of PTCDA:CuPc films with and without C_{60} film. And AFM images of **c** C_{60}/PTCDA:CuPc and **d** PTCDA:CuPc films

show strong light absorption in the spectrum range of 200–400 nm and a uniform light absorption in the spectrum range of 450–700 nm. It is worth noting that a remarkably enhanced absorption was found from 200 to 500 nm when different thickness C_{60} films were inserted between the interface of the quartz glasses and PTCDA:CuPc films, which could be attributed to the absorption of C_{60} film dominates in the spectrum range of 200–500 nm. Figure 2b–d shows the XRD and AFM images of PTCDA:CuPc on 10 nm C_{60} film and single PTCDA:CuPc film. The double layer show an additional peak at 31.9°. As shown in the AFM images, the surface of the PTCDA:CuPc film is similar with or without the C_{60} layer. However, the roughness of the photosensitive film on the C_{60} layer is slightly higher. This shows that the addition of C_{60} does not significantly improve the performance of the device optically, or even not at all. Therefore, we believe that the improvement of device performance comes from the hole blocking effect of C_{60}.

The crystallite size (D) can be calculated by

$$D = k\lambda/(\beta \cos\theta), \tag{1}$$

where k is a constant, equal to 0.89, λ is X-ray wavelength of 0.15405 nm, β is full width at half maxima (FWHM) of

diffraction peak, θ is diffraction angle. The FWHM of the peak at $2\theta = 31.9$ is 0.1617°. The calculated crystallite size is about 50 nm, which is consistent with the AFM image.

Figure 3a shows the typical *I–V* characteristics of the OIHPDs based on bulk heterojunction without C_{60} in the dark and under illumination of 532 nm laser. It is clear that the dark current is a bit large at a reverse bias voltage of − 10 V, which is as high as 1615.9 μA. The dependences of photocurrent on the reverse bias voltage are shown in Fig. 3b. It is seen that the photocurrent increases obviously with the incident optical power and gradually becomes saturated with reverse bias voltage increasing, which exhibits standard photodiode characteristics.

As an important parameter of photodetectors, the photoresponsivity (R) is defined as the value of the photocurrent (I_{ph}) which generated in the external circuit under illumination of unit incident optical power (P_{in}), that is [39]

$$R = \frac{I_{ph}}{P_{in}}. \tag{2}$$

Another important parameter characterizing photodetectors is the specific detectivity (D^*). Here we ignore the power spectral density of other noise sources such as flicker or thermal noise, it can be described as [40]

$$D^* = \frac{R}{\sqrt{2qJ_{dark}}}, \tag{3}$$

where q is the elementary electric charge, J_{dark} is the dark current density.

Figure 4a shows the dependence of photoresponsivity R on the wavelength at a reverse bias voltage of − 10 V and an incident optical power of ~ 0.1 mW. In the broad spectral response range from 405 to 808 nm, the responsivities of the OIHPD without C_{60} film (C_{60}-free OIHPD) are all greater than 0.68 A/W. Especially, at the wavelength of 655 nm, the highest responsivity value is as high as 2.57 A/W. In addition, photoresponsivity generally follows the absorption spectrum of heterojunction films. As shown in Fig. 4b, under different wavelengths of light, the photoresponsivity decreased linearly with the incident light power increased in the logarithmic coordinate. Moreover, the maximal photoresponsivity is 8.13 A/W under 655 nm wavelength illumination with an incident optical power of 0.003 mW, and the minimal photoresponsivity is 0.32 A/W under 808 nm wavelength illumination with an incident optical power of 3.29 mW.

Figure 5 shows the *I–V* characteristics of the OIHPDs with different thicknesses C_{60} films (C_{60}-OIHPDs) in the dark and under 532 nm laser illumination. All measurements were conducted in the same reverse bias voltage range with different incident optical power. It is observed that the dark currents were 92.1 μA (Fig. 5a), 25.6 μA (Fig. 5b), 149.0 μA (Fig. 5c) and 179.8 μA (Fig. 5d), which corresponded to the C_{60} thickness of 5 nm, 10 nm, 20 nm, 30 nm, respectively. Additionally, the C_{60}-OIHPDs exhibited much lower dark current (Fig. 3a vs Fig. 5), and the minimum dark current of C_{60}-OIHPDs was 25.6 μA when the C_{60} film thickness is 10 nm, which is about 63 times smaller than it of the C_{60}-free OIHPD. Moreover, it is interesting to find that the dark current decreased first and then increased with increasing C_{60} thickness. Considering the energy level, a mechanism explanation as shown in Fig. 6 is proposed to support the phenomenon of the above OIHPDs. It is noteworthy that the energy levels of valence band (E_v) (5.24 eV) of p-type silicon, the highest occupied molecular orbital (HOMO) (5.3 eV) of

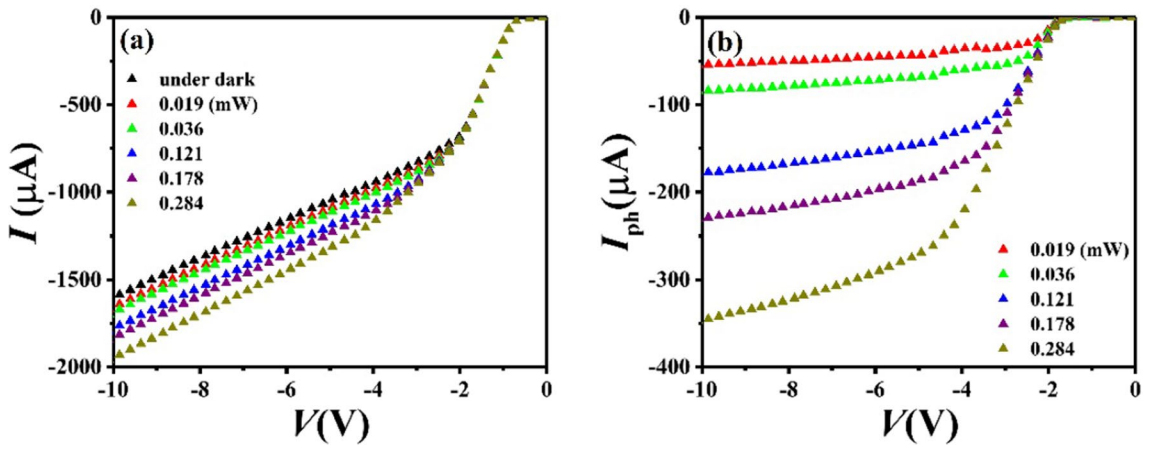

Fig. 3 **a** The *I–V* characteristics of the device Si/PTCDA:CuPc (30 nm)/Au in the dark and under 532 nm laser illumination with different optical power. **b** The dependences of photocurrent on the reverse bias voltage under 532 nm laser illumination with different optical power

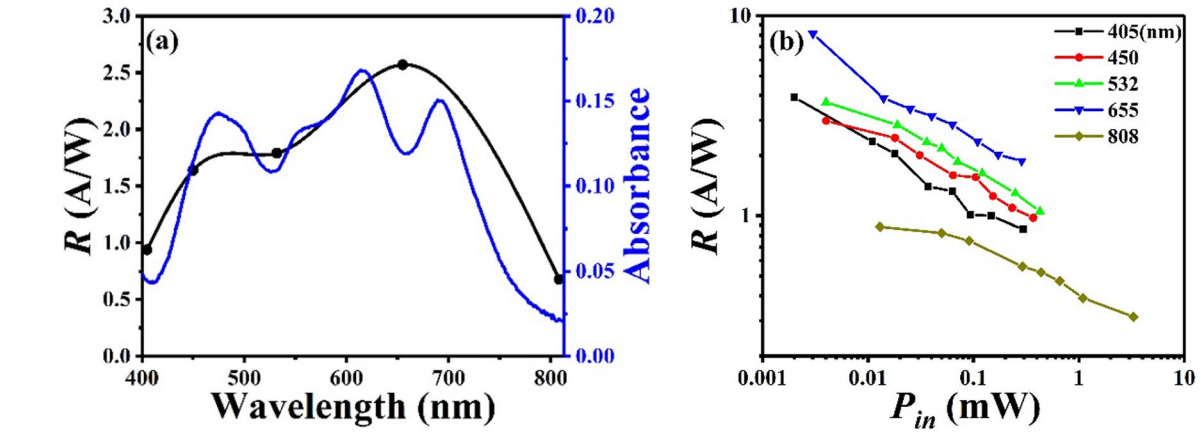

Fig. 4 **a** The dependence of photoresponsivity *R* on the wavelength. **b** The logarithmic dependences of *R* on the incident optical power P_{in}. All results were obtained at a reverse bias voltage of − 10 V and an incident optical power of ~ 0.1 mW

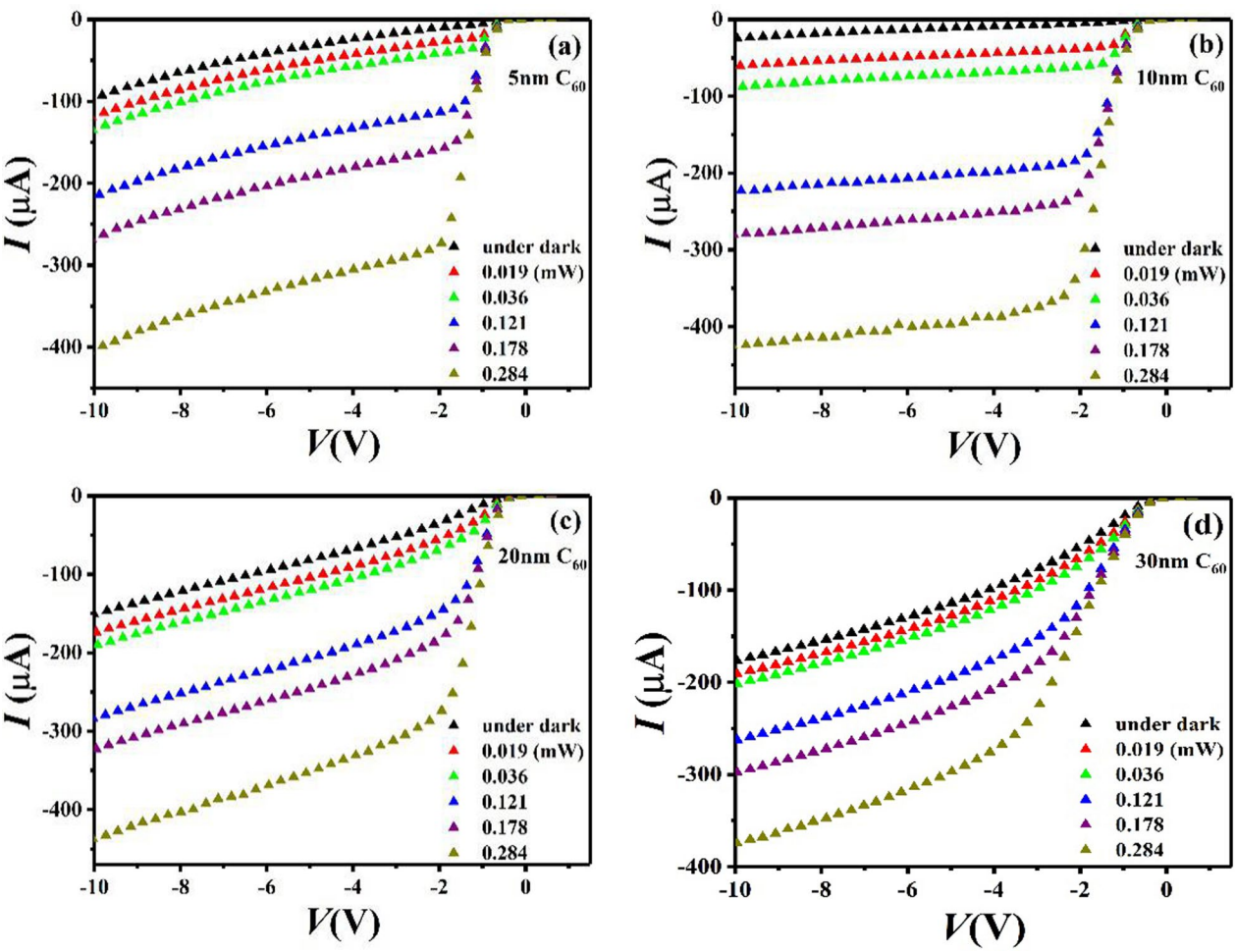

Fig. 5 The *I*–*V* characteristics of the device Si/C_{60}/PTCDA:CuPc (30 nm)/Au in the dark and under 532 nm laser illumination with different optical power. The thicknesses of C_{60} films are **a** 5 nm, **b** 10 nm, **c** 20 nm and **d** 30 nm, respectively

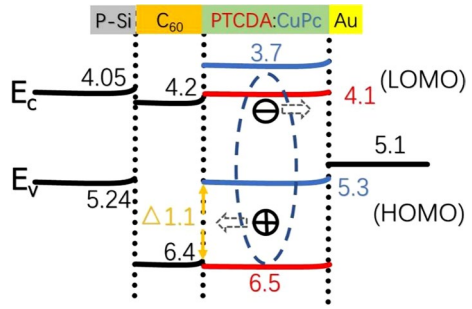

Fig. 6 The energy level diagram and charge generation kinetics and transport mechanisms

CuPc and the work function of the gold electrode (5.1 eV) match well for hole transport in the absence of the C_{60} layer. Therefore, the holes can reach p-type silicon easily under a very low voltage bias, which causes a large dark current in the C_{60}-free OIHPD. Fortunately, the HOMO (6.4 eV) of C_{60} is higher than the HOMO (5.3 eV) of CuPc, which means it will match better ($\Delta = 1.1$ eV) for blocking hole transport. This is consistent with the experimental results that a high dark current of 1615.9 μA in the C_{60}-free OIHPD and a low current of 25.6 μA in the C_{60}-OIHPD. However, as an excellent electron transport material with high electron mobility (> 1.3 cm^2 V^{-1} s^{-1}) [41], a small amount of electrons can still easily reach the lowest occupied molecular orbital LUMO (4.2 eV) of C_{60} from the guide band E_c (4.05 eV) of p-type silicon. Thus, as the thickness of C_{60} film increasing, we infer that the injection of electrons is enhanced. In this regard, it has been reported that the strain relaxation in the multilayer film is related to the film thickness [42, 43]. Consequently, it is reasonable to assume that a thicker C_{60} film can provide broader space for the multilayer film, thereby more effectively alleviating the interplanar stress. In addition, the promotion of electron transport by the C_{60} film has become the dominant factor affecting dark current, which may be due to the increase of the dark current when the thickness of the C_{60} film exceeds 10 nm.

In order to better understand the effects of C_{60} thickness on device performance, the relationship curves about the dependences of photoresponsivity R on the thickness of C_{60} films is plotted in Fig. 7a. Under the wavelength of 405–532 nm, there is an overall trend that R firstly increased and then decreased with C_{60} thickness increasing, and the maximum value of R was reached with 10 nm thick C_{60} film. It is indicated that C_{60} film does enhance optional absorption from 200 to 500 nm, which is consistent with the absorption spectrum of C_{60} single layer (Fig. 2). But the thicker C_{60} film will also lead to smaller photocurrent and smaller R, this is probably because C_{60} film hinders the transmission of portion of the photogenerated carriers. As for the wavelength of 450–532 nm, R significantly decreased when the thickness of C_{60} increasing from 0 to 5 nm, we speculate that the inhibitory effect of the C_{60} film on the photocurrent is greater than the enhancement effect at this time. Under the wavelength of 655–808 nm, R decreased continuously as the thickness of C_{60} increasing, since the C_{60} film has no significant enhancement effect at the wavelength of 655–808 nm. Figure 7b shows the dependences of D^* on the thickness for different wavelengths. The D^* of device under different wavelengths illumination firstly increased with C_{60} thickness increasing and reach a maximum

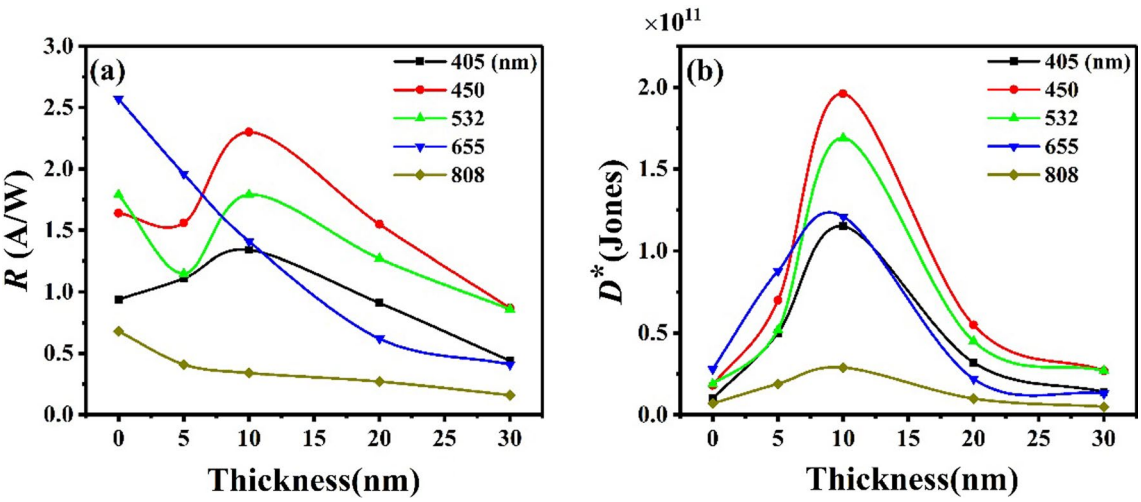

Fig. 7 The dependences of **a** photoresponsivity R on the different C_{60} thicknesses, **b** specific detectivity D^* on the thickness for different wavelengths. All results were obtained at a reverse bias voltage of − 10 V and an incident optical power of ~ 0.1 mW

value at 10 nm, then decreased. The results above manifest that the optimized C_{60} thickness is 10 nm, which makes the D^* reach the maximum. For the OIHPD with 10 nm C_{60} film (10 nm-C_{60} OIHPD), the D^* over 10^{11} Jones in the wavelength range of 405–655 nm, and the highest D^* value is 1.96×10^{11} under the illumination of 450 nm wavelength. Compared with C_{60}-free OIHPD, the D^* of 10 nm-C_{60} OIHPD is almost one order of magnitude larger in the wavelength range of 405–808 nm (details in Table 1).

Figure 8a shows the dependence of photoresponsivity R on the wavelength for an incident optical power of ~ 0.1 mW at − 10 V. It is worth mentioning that the peak value of responsivity of 10 nm-C_{60} OIHPD changes to around 450 nm from 655 nm of C_{60}-free OIHPD (Fig. 8a vs Fig. 4a) due to the addition of C_{60} film, which enhanced the absorption spectrum from 200 and 500 nm (Fig. 2). Furthermore, significantly reduced responsivity values are obtained at the wavelength of 655 nm and 808 nm (Fig. 8a vs Fig. 4a) due to C_{60} film which hinders the transmission of portion of the photo-generated carriers. As shown in Fig. 8b, it is seen that the 10 nm-C_{60} OIHPD has the best responsivity under the illumination of 450 nm because of the influence of C_{60} film. And the maximal responsivity is 4.53 A/W at an incident optical power of 0.004 mW of 450 nm, the minimal responsivity is 0.30 A/W at an incident optical power of 3.29 mW of 808 nm, respectively.

Conclusion

In summary, the photodiodes based on hybrid planar-bulk heterojunction with different thicknesses C_{60} films were fabricated and characterized. The broad spectral region response from visible to near-infrared demonstrated that using C_{60} films as hole-blocking layer can effectively enhance the performance of broad spectral OIHPDs. Specifically, the OIHPD with 10 nm-C_{60} film exhibited the optimized performance with a much lower dark current of 25.6 μA, which is about 63 times smaller than that of C_{60}-free OIHPD. A schematic energy level model combined with experimental measurements is well capable of explaining the origin

Table 1 Comparison of the photosensitive performance of broad spectral OIHPDs with different C_{60} thicknesses

Device											
C_{60} thickness	R (AW^{-1})[a]					D^* ($\times 10^{11}$ Jones)[a]					I_{dark} (μA)[a]
Wavelength (nm)	405	450	532	655	808	405	450	532	655	808	
0-nm	0.94	1.64	1.79	2.57	0.68	0.10	0.18	0.19	0.28	0.07	1615.0
5-nm	1.11	1.56	1.15	1.96	0.41	0.50	0.70	0.52	0.88	0.19	92.1
10-nm	1.34	2.30	1.97	1.41	0.34	1.15	1.96	1.69	1.21	0.29	25.6
20-nm	0.91	1.55	1.27	0.62	0.27	0.32	0.55	0.45	0.22	0.10	149.0
30-nm	0.44	0.87	0.86	0.41	0.16	0.14	0.28	0.28	0.13	0.05	179.8

[a] All results were obtained at a reverse bias voltage of − 10 V and an incident optical power of ~ 0.1 mW

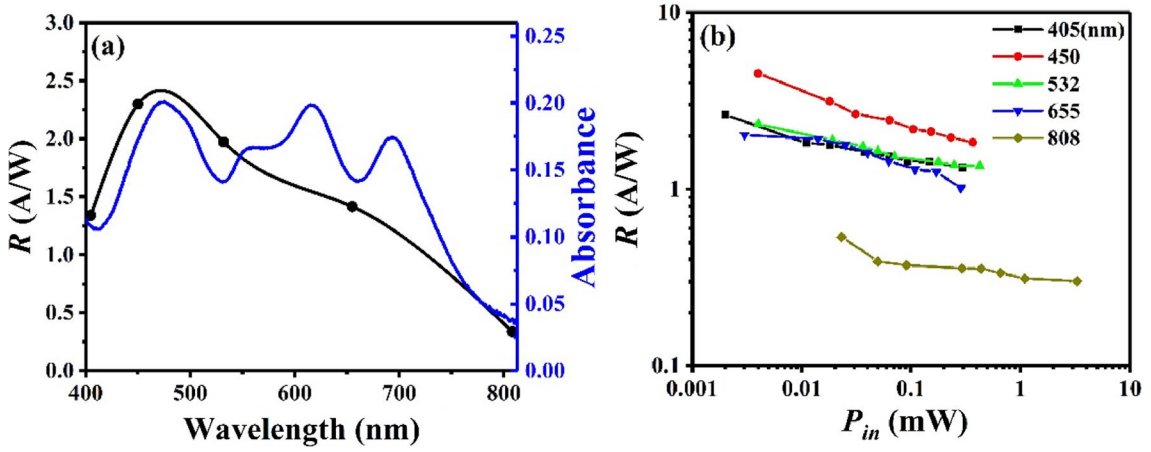

Fig. 8 **a** The dependence of photoresponsivity R on the wavelength. **b** The logarithmic dependences of R on the incident optical power P_{in}. All results were obtained at a reverse bias voltage of − 10 V and an incident optical power of ~ 0.1 mW

of decreased dark current. Furthermore, the D^* of the 10 nm-C_{60} OIHPD was almost one order of magnitude larger than the C_{60}-free photodiode, and a notable enhancement of over 10^{11} Jones was obtained due to the fiercely reduced dark current.

Abbreviations

OIHPD: Organic–inorganic hybrid photodiode; PTCDA: 3,4,9,10-Perylenetetracarboxylic dianhydride; CuPc: Copper phthalocyanine; C_{60}: Fullerene; TAPC: 1,1-Bis ((di-4-tolylamino) phenyl) cyclohexane; *EQE*: External quantum efficiency; D^*: Specific detectivity; *R*: Photoresponsivity; XRD: Diffraction of x-rays; FWHM: Full width at half maxima; AFM: Atomic force microscope.

Acknowledgements

Not applicable.

Authors' contributions

ZZ: experiment, writing, GL: experiment, writing, XS: experiment, QD: experiment, LS: corresponding author, YP: corresponding author, PW: experiment instructor. All authors read and approved the final manuscript.

Funding

This work was supported by Natural Science Foundation of Zhejiang Province Grant No. LQ20F050008.

Availability of data and materials

The data in the manuscript were obtained from our measurements, so we will not share the data.

Declarations

Competing interests

The authors declare that they have no competing interests.

Author details

[1]College of Optical and Electronic Technology, China Jiliang University, Hangzhou 310018, China. [2]Institute of Microelectronics, School of Physical Science and Technology, Lanzhou University, Lanzhou 730000, China.

Received: 22 June 2021 Accepted: 30 December 2021
Published online: 25 January 2022

References

1. Vijay J, Yadav RK, Alvi PA, Singh K, Rathi A (2020) Design and modeling of InGaAs/GaAsSb nanoscale heterostructure for application of optical fiber communication system. Mater Today Proc.
2. Rutz F, Bächle A, Aidam R, Niemasz J, Bronner W, Zibold A, Rehm R, Fulop GF, Hanson CM, Andresen BF (2019) InGaAs SWIR photodetectors for night vision. Infrared Technol Appl XLV 37
3. Ren D, Azizur-Rahman KM, Rong Z, Juang BC, Somasundaram S, Shahili M, Farrell AC, Williams BS, Huffaker DL (2019) Room-temperature mid-wavelength infrared InAsSb nanowire photodetector arrays with Al_2O_3 Passivation. Nano Lett 19(5):2793–2802
4. Benavides CM, Biele M, Schmidt O, Brabec CJ, Tedde SF (2018) TIPS Pentacene as a beneficial interlayer for organic photodetectors in imaging applications. IEEE Trans Electron Dev 65:1516–1522
5. Lien MB, Liu CH, Chun IY, Ravishankar S, Nien H, Zhou M, Fessler JA, Zhong Z, Norris TB (2018) Ranging and light field imaging with transparent photodetectors. Nat Photon 1–6
6. Wang B, Zhong S, Ge Y, Wang H, Luo X, Zhang H (2020) Present advances and perspectives of broadband photo-detectors based on emerging 2D-Xenes beyond grapheme. Nano Res 13(4):891–918
7. Xiao M, Mingyu L, Jian-Jun H (2013) CMOS-compatible integrated spectrometer based on echelle diffraction grating and MSM photodetector array. IEEE Photon J 5:6600807–6600807
8. Shi L, Nihtianov S (2012) Comparative study of silicon-based ultraviolet photodetectors. IEEE Sens J 12:2453–2459
9. Xu GY, Salvador A, Kim W, Fan Z, Lu C, Tang H, Morkoç H, Smith G, Estes M, Goldenberg B, Yang W, Krishnankutty S (1997) High speed, low noise ultraviolet photodetectors based on GaN p-i-n and AlGaN(p)-GaN(i)-GaN(n)structures. Appl Phys Lett 71:2154–2156
10. Kimukin I, Biyikli N, Butun B, Aytur O, Unlu MS, Ozbay E (2002) InGaAs-based high-performance p-i-n photodiodes. IEEE Photonic Tech L 14:366–368
11. Yoshizawa A, Tsuchida H (2001) A 1550 nm single-photon detector using a thermoelectrically cooled InGaAs avalanche photodiode. Jpn J Appl Phys 40:200–201
12. Li YN, Sonar P, Murphy L, Hong W (2013) High mobility diketopyrrolopyrrole (DPP)-based organic semiconductor materials for organic thin film transistors and photovoltaics. Energy Environ Sci 6:1684–1710
13. Katz HE, Lovinger AJ, Johnson J, Kloc C, Siegrist T, Li W, Lin YY, Dodabalapur A (2000) A soluble and air-stable organic semiconductor with high electron mobility. Nature 404:478–481
14. Costa JCS, Taveira RJS, Lima CFRAC, Mendes A, Santos LMNBF (2016) Optical band gaps of organic semiconductor materials. Opt Mater 58:51–60
15. Dailey S, Feast WJ, Peace RJ, Sage IC, Till S, Wood EL (2001) Synthesis and device characterisation of side-chain polymer electron transport materials for organic semiconductor applications. J Mater Chem 11:2238–2243
16. Rim YS, Yang YM, Bae SH, Chen H, Li C, Goorsky MS, Yang Y (2015) Ultrahigh and broad spectral photodetectivity of an organic-inorganic hybrid phototransistor for flexible electronics. Adv Mater 27:6885–6891
17. Zhao F, Luo X, Liu J, Du L, Lv W, Sun L, Li Y, Wang Y, Peng Y (2016) Toward high performance broad spectral hybrid organic–inorganic photodetectors based on multiple component organic bulk heterojunctions. J Mater Chem C 4:815–822
18. Yang DZ, Zhou XK, Wang YP, Vadim A, Alshehri SM, Ahamad T, Ma DG (2016) Deep ultraviolet-to-NIR broad spectral response organic photodetectors with large gain. J Mater Chem C 4:2160–2164
19. Wang W, Zhao D, Zhang F, Li L, Du M, Wang C, Yu Y, Huang Q, Zhang M, Li L, Miao J, Lou Z, Shen G, Fang Y, Yan Y (2017) Highly sensitive low-bandgap perovskite photodetectors with response from ultraviolet to the near-infrared region. Adv Funct Mater 27:1703953
20. Han J, Yang D, Ma D, Qiao W, Wang ZY (2019) Preparation of AZO:PDIN hybrid interlayer materials and application in high-gain polymer photodetectors with spectral response from 300 nm to 1700 nm. Org Electron 68:242–247
21. Ma L, Fan H, Tian H, Fang J, Qian X (2016) The n-ZnO/n-In_2O_3 heterojunction formed by a surface-modification and their potential barrier-control in methanal gas sensing. Sens Actuators B Chem 222:508–516
22. Zhang M, Fan H, Zhang N, Peng H, Ren X, Wang W, Li H, Chen G, Zhu Y, Jiang X, Wu P (2018) 3D hierarchical $CoWO_4$/Co_3O_4 nanowire arrays for asymmetric supercapacitors with high energy density. Chem Eng J 347:291–300
23. Tian H, Fan H, Li M, Ma L (2016) Zeolitic imidazolate framework coated ZnO nanorods as molecular sieving to improve selectivity of formaldehyde gas sensor. ACS Sens 1:243–250
24. Huang F, Li Y, Xia H, Zhang J, Xu K, Peng Y, Liu G (2017) Towards high performance broad spectral response fullerene based photosensitive organic field-effect transistors with tricomponent bulk heterojunctions. Carbon 118:666–674
25. Huang F, Wang X, Xu K, Liang Y, Peng Y, Liu G (2018) Broadband organic phototransistor with high photoresponse from ultraviolet to near-infrared realized via synergistic effect of trilayer heterostructure. J Mater Chem C 6:8804–8811
26. Peng Y, Huang F, Zhang J, Luo X, Xu K, Lv W, Xu S, Wang Y, Tang Y, Wei Y, Xu Z, Yang Y, Lu F (2017) Broad spectral response photosensitive organic field-effect transistors realized by the hybrid planar-bulk heterojunction composed of three molecules with complementary optical absorption. Org Electron 43:27–32
27. Tchernycheva M, Guan N, Dai X, Messanvi A, Zhang H, Bayle F, Neplokh V, Piazz V, Julien FH, Bougerol C, Vallo M, Durand C, Eymery J (2016) Flexible optoelectronic devices based on nitride nanowires embedded in

polymer films. In; IEEE nanotechnology materials and devices conference (NMDC), pp 1–2
28. Huang J, Du J, Cevher Z, Ren Y, Wu X, Chu Y (2017) Printable and flexible phototransistors based on blend of organic semiconductor and biopolymer. Adv Funct Mater 27:1604163
29. Pierre A, Arias AC (2016) High-detectivity printed organic photodiodes for large area flexible imagers. IEEE international electron devices meeting
30. Gelinck GH, Kumar A, Moet D, van der Steen JLPJ, van Breemen AJJM, Shanmugam S, Langen A, Gilot J, Groen P, Andriessen R, Simon M, Ruetten W, Douglas AU, Raaijmakers R, Malinowski PE, Myny K (2016) X-ray detector-on-plastic with high sensitivity using low cost, solution-processed organic photodiodes. IEEE Trans Electron Devices 63:197–204
31. Qian C, Sun J, Kong L-A, Gou G, Zhu M, Yuan Y, Huang H, Gao Y, Yang J (2017) High-performance organic heterojunction phototransistors based on highly ordered copper phthalocyanine/para-sexiphenyl thin films. Adv Funct Mater 27:1604933
32. Shekhar H, Solomeshch O, Liraz D, Tessler N (2017) Low dark leakage current in organic planar heterojunction photodiodes. Appl Phys Lett 111:223301
33. Ma C, Shi Y, Hu W, Chiu MH, Liu Z, Bera A, Li F, Wang H, Li LJ, Wu T (2016) Heterostructured $WS_2/CH_3NH_3PbI_3$ photoconductors with suppressed dark current and enhanced photodetectivity. Adv Mater 28:3683–3689
34. Park S, Kim SJ, Nam JH, Pitner G, Lee TH, Ayzner AL, Wang H, Fong SW, Vosgueritchian M, Park YJ, Brongersma ML, Bao Z (2015) Significant enhancement of infrared photodetector sensitivity using a semiconducting single-walled carbon nanotube/C_{60} phototransistor. Adv Mater 27:759–765
35. Li Y, Lv W, Luo X, Sun L, Zhao F, Zhang J, Zhong J, Huang F, Peng Y (2015) Enhanced performance of PbPc photosensitive organic field effect transistors by inserting different-thickness pentacene inducing layers. Org Electron 26:186–190
36. Luo X, Du L, Wen Z, Lv W, Zhao F, Jiang X, Peng Y, Sun L, Li Y, Rao J (2015) Remarkably enhanced red-NIR broad spectral absorption via gold nanoparticles: applications for organic photosensitive diodes. Nanoscale 7:14422–14433
37. Yim C, McEvoy N, Riazimehr S, Schneider DS, Gity F, Monaghan S, Hurley PK, Lemme MC, Duesberg GS (2018) Wide spectral photoresponse of layered platinum diselenide-based photodiodes. Nano Lett 18:1794–1800
38. Ni Z, Ma L, Du S, Xu Y, Yuan M, Fang H, Wang Z, Xu M, Li D, Yang J, Hu W, Pi X, Yang D (2017) Plasmonic silicon quantum dots enabled high-sensitivity ultrabroadband photodetection of graphene-based hybrid phototransistors. ACS Nano 11:9854–9862
39. Peng Y, Ding R, Ren Q, Xu S, Sun L, Wang Y, Lu F (2018) High performance photodiode based on MoS2/pentacene heterojunction. Appl Surf Sci 459:179–184
40. Lv W, Peng Y, Zhong J, Luo X, Li Y, Zheng T, Tang Y, Du L, Peng L (2015) Near infrared sensitive organic photodiode utilizing exciplex absorption in $NdPc_2/C_{60}$ heterojunction. IEEE Photon Technol Lett 19:1–1
41. Dong G, Zheng H, Duan L, Wang L, Qiu Y (2009) High-performance organic optocouplers based on a photosensitive interfacial C_{60}/NPB heterojunction. Adv Mater 21:2501–2504
42. Tamulevicius S (1998) Stress and strain in the vacuum deposited thin films. Vacuum 51:127–139
43. Abermann R (1990) Measurements of the intrinsic stress in thin metal-films. Vacuum 41:1279–1282

Publisher's Note

Springer Nature remains neutral with regard to jurisdictional claims in published maps and institutional affiliations.

Submit your manuscript to a SpringerOpen journal and benefit from:

- ► Convenient online submission
- ► Rigorous peer review
- ► Open access: articles freely available online
- ► High visibility within the field
- ► Retaining the copyright to your article

Submit your next manuscript at ► springeropen.com